

Stoichiometry and Termination Control of LaAlO₃/SrTiO₃ Bilayer Interfaces

Hong Yan[§], Jacqueline Marie Börgers[§], Marc-André Rose, Christoph Baeumer,

*Bongju Kim, Lei Jin, Regina Dittmann, and Felix Gunkel**

[§]equal contributions

Dr. H. Yan, J. M. Börgers, M. Rose, Prof. R. Dittmann, Dr. F. Gunkel
Peter Grünberg Institut 7 and JARA-FIT, Forschungszentrum Jülich, Jülich, 52425,
Germany
E-mail: f.gunkel@fz-juelich.de

M. Rose, Dr. C. Baeumer, Dr. F. Gunkel
Institute for Electronic Materials (IWE 2), RWTH Aachen University, Aachen, 52062,
Germany

Prof. Dr. B. J. Kim
Department of Energy Science, Sung Kyun Kwan University, Gyeonggi-do, 16419,
Korea

Dr. L. Jin
Ernst Ruska-Centre for Microscopy and Spectroscopy with Electrons (ER-C) and
JARA-FIT, Forschungszentrum Jülich GmbH, Jülich, 52425, Germany

J. M. Börgers
Current address: Institute of Physical Chemistry, RWTH Aachen University, Aachen,
52056, Germany

Dr. F. Gunkel
Current address: Department of Energy Conversion and Storage (DTU Energy),
Technical University of Denmark, DK-2800 Kgs. Lyngby, Denmark

Keywords: two-dimensional electron gases, SrTiO₃ thin films, electronic transports,
atomically tailored materials, emerging interface properties

* Author to whom correspondence should be addressed; electronic-mail: f.gunkel@fz-juelich.de

Abstract

Driven by the interest in fundamental physics and potential applications in novel electronic devices, intense effort is devoted to integration of oxide-based two-dimensional electron gases (2DEGs) with other functional materials. As a classic model system, $\text{LaAlO}_3/\text{SrTiO}_3$ (LAO/STO) has gained significant attentions. However, due to limitations in synthesis and high demands on the involved thin films, the formation of conductive interfaces between artificially grown STO and LAO thin films is an extreme challenge: oftentimes these interfaces remain insulating or show poor transport properties, which inhibits the development of all-thin-film devices. Here, by adopting high temperature growth to achieve step-flow growth mode and fine-tuning the laser fluence during pulsed laser deposition, high quality homoepitaxial STO thin films with sufficiently low point-defect concentration and controllable surface termination are obtained. Fully metallic 2DEGs are then realized at interfaces between STO thin films and both crystalline and amorphous LAO overlayers. The observed slightly reduced mobility in the bilayer LAO/STO/STO structures as compared with single-layer LAO/STO structure is related to the residual defect formation during STO synthesis, yielding a disordered metallic oxide system. The results give prospect of multilayer interfaces potentially accessible in superlattice structures and provide a reliable starting point for back-gated all-thin-film field-effect devices.

1. Introduction

Complex oxides are particularly appealing for advances in device technology due to a range of remarkable functional material properties, such as colossal magnetoresistance and high temperature superconductivity.^[1-4] Currently, intense research effort is devoted to exploring the emergent properties and potential applications of interfaces between dissimilar oxide materials.^[5,6] At the interfaces, one can exploit not only incorporated materials, but also new emergent properties that are inherent to the specific interface.^[7,8] A particular example in this area is the observation of metallic conductivity at the interface between the two insulators LaAlO_3 (LAO) and SrTiO_3 (STO).^[9,10] This interface exhibits a broad spectrum of remarkable physical properties, such as high electron mobility,^[9,11] ferromagnetism,^[12] and field-tunable superconductivity,^[13] which are promising for the integration of new functionalities into electronics and spintronics applications. The interfacial metallic state is often explained by the polarity-mismatch, which results in a potential build-up and subsequent charge-transfer across the interface.^[9,14] The other two mainstream viewpoints are the formation of oxygen vacancies,^[15,16] and La/Sr short-range interdiffusion.^[17,18] Details about the effects of defects on the properties of such oxide interfaces, such as electronic states are, however, still under discussion.^[19-23]

Driven by the interest in fundamental physics and possible future applications for novel electronic devices, efforts have been made to integrate the two-dimensional electron gas (2DEG) with other functional materials.^[24-28] This approach opens the

possibility of investigating strain and defect effects.^[27-29] Therefore, the single crystalline STO substrate which is used as a standard to achieve 2DEG-heterostructures, is replaced by a STO thin film, transferring the conductive interface from well-defined single crystalline substrates to an artificially grown thin film. This task poses a huge challenge due to the high demands on the quality of thin films for the formation of 2DEGs.^[9,26,30] The first step towards transferring the functional LAO/STO interface into more complex device structures is to achieve a 2DEG with metallic, interfacial transport properties onto a homoepitaxial STO thin film. While this appears to be a trivial task using state-of-the-art oxide epitaxy, it turns out to be a remarkable challenge in the field.^[29,31,32]

For one, a crucial prerequisite is the TiO₂-termination of the STO at the interface, which is essential to obtain charge-transfer from crystalline LAO into STO and determines the dynamics of the generation of oxygen vacancies with view on amorphous LAO.^[9,30,33,34] A common route for atomically defined termination is the chemical treatment of single crystalline substrates.^[35] During thin film synthesis, however, the chemical termination of the growing layer is not necessarily well-conserved. Secondly, point defects inside the growing STO layer typically act as trapping centers for electrons, particularly point-defects on cation sites arising from slight cation non-stoichiometry during the growth.^[32,36-39] Therefore, the amount of point defects incorporated in the STO layer during growth needs to be as low as possible.^[32]

Until now, most attempts to transfer the LAO/STO interfaces onto another substrate

have resulted in insulating LAO/STO interfaces. In some cases where a conductive interface was achieved,^[27-29,32,40-43] it showed limited performance (as indicated e.g. by a considerably lowered electron mobility, of order of $10 \text{ cm}^2/\text{Vs}$) and non-metallic low-temperature behavior (i.e. strong resistance upturns in the low-temperature regime).^[27-29,32] Moreover, the thickness of the epitaxial STO thin film in some of these cases was restricted to the nanometer range.^[26] For the application of such heterostructures in real electronic devices, such as all-thin-film backgated field-effect devices, larger thicknesses may be required in order to overcome electrostatic screening lengths and to avoid overlapping space charge layers.^[44,45]

In general, homoepitaxy of SrTiO_3 with high quality and precision was already demonstrated in the pioneering work of Kawasaki et al.^[46] and is today widely accessible by means of PLD and MBE. However, the control of point defect concentrations and particularly the control of surface termination of the growing film is still a well-debated topic.^[34,36,37] While termination control is ultimately accessible in MBE,^[27,28] the concomitant supply of A-site and B-site cations in pulsed laser deposition poses additional complexity to determining and controlling the resulting surface termination of the thin film. For instance, in the early work by Kawasaki et. al. it was observed that homoepitaxial STO typically results in SrO-termination,^[46] which would not provide the required template for 2DEG formation. On the other hand, various publications did report on successful growth of LAO/STO bilayer interfaces, implying successful fabrication of TiO_2 -terminated interfaces. Typically, however, additional etching and heat treatments of the SrTiO_3 thin films were

necessary.^[27,28] Moreover, often only a limited metallicity and low electron mobility is observed, as discussed above and demonstrating a need to further improve and lower the defect density in SrTiO₃ thin films.

In this work, we demonstrate the fabrication of homoepitaxial STO thin films with well-matched stoichiometry and defined surface termination, which can be controlled via growth-mode control and tuning of the deposition parameters. In particular, we adopted high laser fluence (F_L) at considerably high oxygen pressure to obtain sufficient stoichiometry and to maintain TiO₂-termination.^[32,36,37] Additionally, we apply increased growth temperature to achieve step-flow growth mode. As we show, key to achieving atomically defined thin films and surfaces is the step-flow growth mode, suitable of providing low point-defect densities and well-defined surface termination. We then demonstrate that 2DEGs are formed at amorphous and crystalline LAO/STO interfaces on our STO thin films, exhibiting metallic behavior down to low temperatures. As we show, the termination control during the growth of STO by fine tuning laser fluence allows to generate interfacial conductivity. Additionally, the step-flow growth mode at high growth temperature is essential to achieve low defect concentration, and thus sufficient electron mobility. A still reduced electron mobility as compared to the single crystal standard indicates a residual amount of scattering centers remaining the STO layers. However, the bilayers allow to study metallic transport in thin film structures with STO layer thicknesses up to 200 nm and to investigate electronic transport phenomena in a disordered, metallic 2D model system. These results provide a systematic recipe for the synthesis of

termination controlled STO layers with comparably low defect concentration, thus, contributing important knowledge to the realization of all-oxide electric field effect devices and to study the fundamental physical properties of 2DEGs on STO.

2. Results

We first address the stoichiometry and termination control during the synthesis of homoepitaxial STO thin films. All films were deposited by pulsed-laser deposition (PLD) and the fabrication process is described in the Experimental Section. In **Figure 1**, the properties of STO layers grown at different temperatures and different laser fluences F_L are shown. Using reflection high-energy electron diffraction (RHEED), we followed the intensity evolution of the specular diffraction spot during the entire growth to identify the growth mode. The recorded RHEED intensity during the initial growth of 200 nm thick STO layers and the corresponding RHEED pattern for the final stage of the growth are shown in Figure 1a. At a temperature of 800 °C (top of

Figure 1a), the STO thin film grows in a layer-by-layer growth mode, resulting in apparently atomically smooth and defined thin film morphology, as indicated by the atomic step-terrace structure observed by atomic force microscopy (AFM) (See Figure S1 in the Supporting Information). A careful optimization of F_L is required to achieve this stable layer-by-layer growth mode towards large layer thicknesses, while a transition to 3D-growth is observed at non-optimum F_L , resulting from Sr rich synthesis (See Figure S1 in the Supporting Information).^[47] At a higher temperature of 950 °C, however, a transition from layer-by-layer to step-flow growth mode is observed, as indicated by the constant RHEED intensity during the growth. This

step-flow growth mode is evident for all F_L applied (Figure 1a, center and bottom).

No transition into 3D growth is observed at any F_L . Moreover, the RHEED diffraction pattern suggests the preservation of 2D morphology after STO growth for all F_L .

Interestingly, the relative change of RHEED intensity between the specular spot (00)

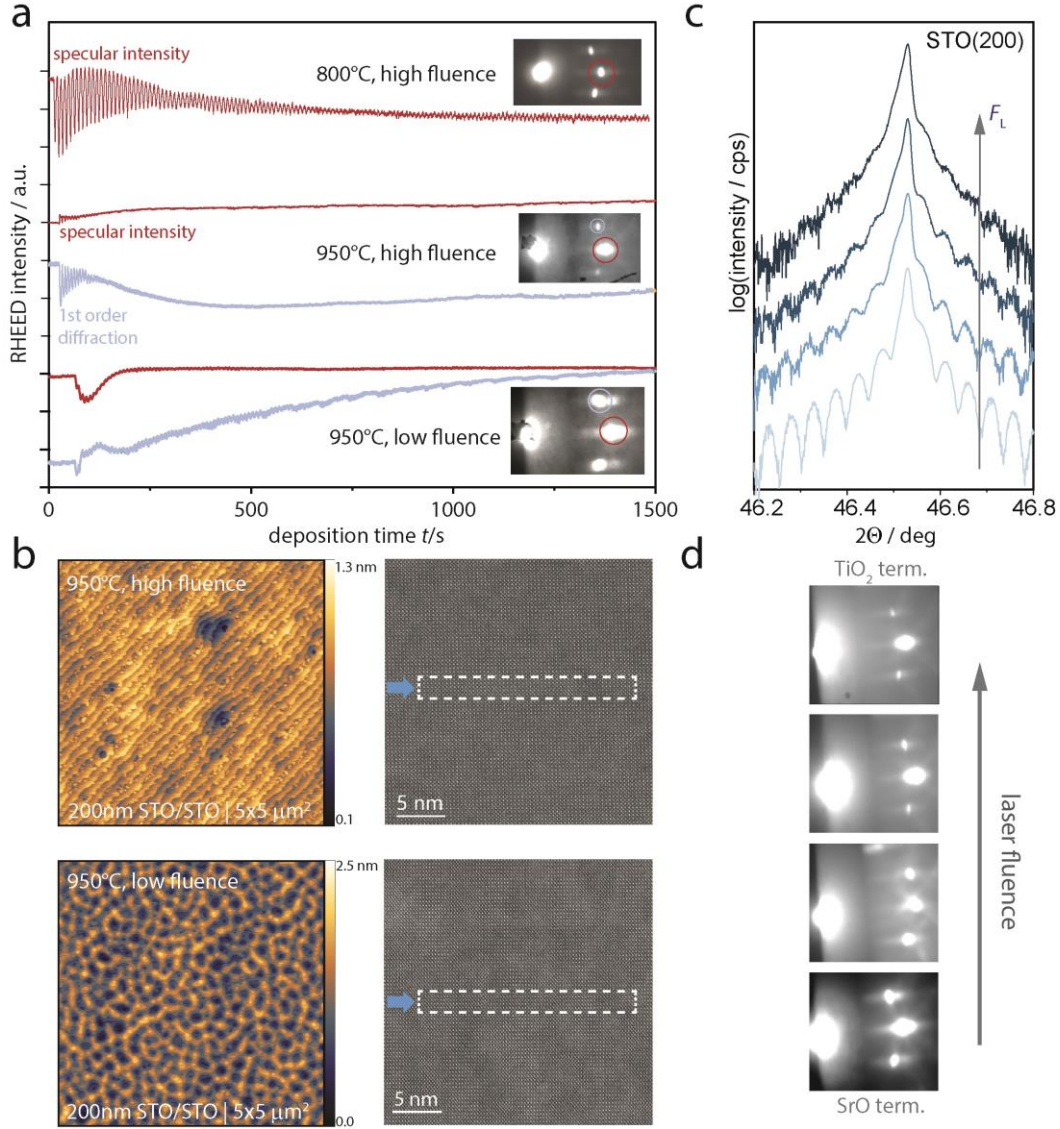


Figure 1. Growth and characterization of STO thin films. a) RHEED intensity oscillations of (0,0) and (10)/(-10) diffraction streaks within the red and light blue circles, respectively, during the first 1500 seconds. Insets show the corresponding RHEED pattern at the end of growth. b) Surface morphology obtained from AFM (left) and corresponding TEM image (right) of STO films grown at 950°C with high and low fluence. In the TEM images, the homoepitaxial interface is marked by an arrows. The white dashed frames serve as guides for the eye. c) XRD-spectra of STO thin films grown at 950°C with increasing laser fluence F_L (indicated by the arrow) in the vicinity of the (200) STO substrate peak. d) RHEED patterns after STO growth at 950°C with increasing F_L .

and the first-order diffracted spots (10) and (-10) are quite different with increasing F_L .

At low F_L (bottom of Figure 1a), increasing intensity of first order diffraction spots (10) and (-10) is observed as compared to the initial stage, eventually exceeding the intensity of the specular reflection. In contrast, for samples grown at high F_L (center of Figure 1a), the intensity of first order diffraction spots remains lower than that of the specular spot during the entire growth process. The evaluation of the RHEED diffraction pattern reflects an extremely surface sensitive technique to determine the atomic structure of the very-surface of the growing film. Therefore, this information can be used to determine the surface-termination of the growing oxide layer. As demonstrated in MBE atomic termination control studies, it was shown that the relative intensity of the first order diffraction in RHEED changes when moving toward SrO and TiO₂ termination.^[48,49] This behavior was attributed to the distinctly different diffraction yields from SrO and TiO₂-terminated surfaces, respectively. In our study, we use this relative intensity change of the 1st order diffraction peak to probe the surface termination of the growing film. Therefore, the two kinds of RHEED patterns observed here are consistent with the ones observed for typical SrO-terminated (at lower F_L) and TiO₂-terminated (at higher F_L) surfaces, respectively.^[34,48,50] These results suggest that high F_L enables a defined TiO₂-termination even after the growth of 200 nm thick STO thin films, while at lower fluences a SrO-termination is preferred. Thus, with the laser fluence we could control primarily the surface termination, which is consistent with a slide

stoichiometry variation of the ablated plasma plume which tends to become more Ti-rich at larger laser fluences.^[51] As a consequence, by slightly Ti-rich growth at high fluences, it is possible to achieve a Ti-terminated surface. Therefore, on the one hand, a high growth temperature triggers the step-flow growth mode, and on the other hand, the laser fluence determines the resulting surface termination.

For the 200 nm thick STO thin films grown in step-flow mode, the surfaces are smooth and show distinct steps with the height of a single unit cell of STO. For high fluences (top of Figure 1b), the surface morphology reveals a smooth surface with clear step terraces and a root-mean-square roughness (R_{RMS}) value of ~ 177.9 pm. For low F_L samples (bottom of Figure 1b), terraces are not visible but all individual steps show the height of a single-unit cell (R_{RMS} ~ 359.2 pm), ~~which is potentially assisted by distinct surface reconstructions of Sr-rich STO surfaces.~~^[49,50] This observation is consistent with previous reports about the morphology of Sr rich (001) STO thin film as determined by *in-situ* AFM.^[52] Thus, the different surface morphologies observed at different laser fluence may potentially be related to different surface termination. Nevertheless, all surfaces can be regarded as flat films with small R_{RMS} values. In general, step-flow growth is expected to show more atomically smooth surface as compared to layer-by-layer growth due to the enhanced mobility of incoming species during the growth associated to this particular growth mode.^[53] We can however conclude that the STO thin films grown with high laser fluence at 800°C and 950°C show comparably similar morphology, while a clear indication of a transition from layer-by-layer growth mode to step-flow growth mode was evident from RHEED

analysis. Note that, the resulting surface termination depends on the chosen F_L . High-angle annular dark-field (HAADF) scanning transmission electron microscopy (STEM) images of the resulting STO/STO interfaces obtained at 950°C show highly coherent thin films. The interface between STO film and substrate is very defined and even hard to be determined on the atomic scale (Figure 1b and Figure S2 for overview images), indicating the absence of significant disorder or secondary phases in the homoepitaxial thin films and their interfaces to the substrate.^[54]

Due to the ionic structure of STO, an increased density of cation vacancies typically results in strain, expanding the c -lattice constant of the thin film.^[36,55,56] In contrast, in ‘absence’ of defects especially cation vacancies, homoepitaxial thin films should adopt the lattice of the substrate in a perfect manner. Therefore, no signature of the thin film would be expected in X-ray diffraction (XRD) measurements. Representative results for (200) peaks are shown in Figure 1c. Next to the (200) Bragg diffraction peak, thickness fringes are observed. These fringes are decreasing in magnitude with increasing F_L to the point that the sample grown with the highest F_L shows almost no fringes. Film and substrate become indistinguishable when F_L is increased indicating stoichiometric growth of STO. Note that also an interfacial distortion of the lattice, as weakly observed in the high-resolution STEM investigation of the low laser fluence thin film can lead to thickness fringes.^[57] The absence of thickness oscillations observed at high laser fluence, hence also indicates the absence of interfacial lattice distortion, consistent with the HAADF STEM analysis (Figure 1b). To conclude, the STO thin films synthesized at high F_L preserve cation

stoichiometry and apparently possess a low defect concentration according to XRD and HAADF STEM analysis. Moreover, according to the RHEED patterns with increasing F_L (Figure 1d) the intensity of the first-order spot is gradually weaker than the ones of the specular spots. Therefore, the STO films grown at 950°C can be assumed to show a transition from SrO terminated to TiO₂ terminated surfaces with increasing fluence.^[34]

We now turn to the question if conducting interfaces can be achieved on the presumably TiO₂ terminated thin films. For this, 10 uc thick LAO layers were grown on the STO thin film surfaces. Their properties are discussed in **Figure 2**. Crystalline LAO layers are growing in layer-by-layer growth mode, as indicated by *in-situ* RHEED (Figure 2a), corroborating that the underlying STO thin film provides atomically defined surfaces. This allows layer-by-layer LAO growth of the bilayer interface, even at a STO layer thickness of 200 nm. An AFM image (Figure 2b) for crystalline LAO layers deposited on a STO thin film with $F_L=2.4 \text{ Jcm}^{-2}$ confirms the preservation of the STO thin film morphology with clear atomic step terraces. Figure

2c shows the room-temperature sheet resistance of the obtained bilayer structures as a function of the F_L used for the STO growth. For samples grown at low F_L , the resistance is above the measurement limit. For samples grown at high F_L , conductive interfaces are observed above a certain fluence threshold. Importantly, at similar film thickness no conductivity was achieved at interfaces to STO thin films grown at 800 °C at any F_L .^[32]

In other studies, LAO/STO bilayer interfaces typically show large and increased

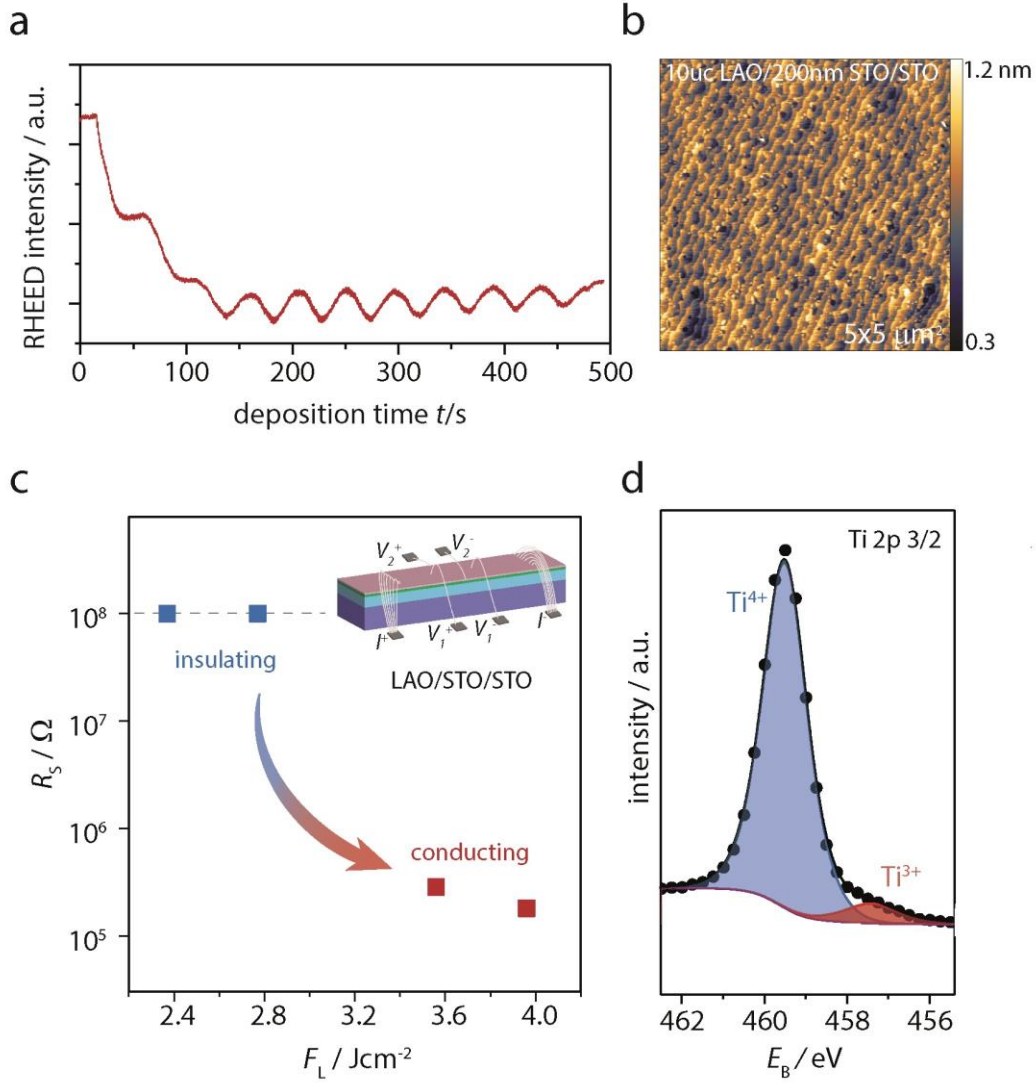


Figure 2. Growth of crystalline LAO on STO thin film and characterization of its interface. a) RHEED intensity oscillations during the deposition of 10 uc LAO on STO thin film with $F_L=2.4 \text{ Jcm}^{-2}$. b) Related surface morphology obtained from AFM. c) Sheet conductance at 300 K for LAO/STO/STO stacks with STO layers grown with different F_L . Inset: A sketch of the LAO/STO/STO sample connected in Hall-bar configuration to measure the sheet resistance and carrier density of the system. d) Ti 2p 3/2 spectra investigated by XPS analysis.

resistance with decreasing temperatures, which is induced by a higher density of scattering centers.^[27,29,32,43] All these studies focused on lower growth temperatures for the respective STO layer implying that the layer-by-layer growth mode achieved at 800°C results in an enhanced defect concentration. This is also in line with previous reports on Nb-doped SrTiO_3 .^[39] Since TiO_2 termination and low defect density are

quite essential for 2DEGs, we obtain no 2DEG in 800°C samples at any F_L . In contrast, the low defect concentration of STO thin films grown at 950 °C seems sufficient for the formation of the 2DEG, but a suitable F_L above the threshold is also required. As suspected based on RHEED in Figure 1, the films grown at high F_L at 950 °C must have TiO₂ termination.

In order to check if the observed conductivity actually stems from the LAO/STO bilayer interface and thus from a 2DEG localized at the interface between the LAO and STO thin films, we applied XPS analysis on the Ti 2*p* core level, as shown in Figure 2d. A clear shoulder occurs due to the occupation of Ti³⁺ states in the vicinity of the LAO/STO interface, which corresponds to about 5 at % of Ti³⁺ in the probed STO volume close to the interface (note that 95% of the XPS intensity comes from the upper 6.9 nm from the surface).^[58] In fact, at such a high concentration of Ti³⁺ in the probed volume, most of the electrons contributing to the observed conductivity must be located within nanometer-distance from the interface. Therefore, it can be confirmed that the 2DEGs-are localized at the bilayer interface between the LAO and STO thin films, and significant conductance contribution originating from the STO substrate or the 200 nm deep STO/STO interface can be excluded.

For a more accurate evaluation of the STO thin films and the formation of the 2DEGs, it is necessary to involve different generation mechanisms of the 2DEG carriers. Therefore, we compared heterostructures with a crystalline LAO overlayer, in which the 2DEG is presumably generated by charge-transfer,^[9] and an amorphous LAO overlayer, where the 2DEG is generated via oxygen-vacancy formation.^[59-62]

Both processes will naturally show a critical thickness phenomenon, as it was shown for standard LAO/STO in the crystalline and amorphous cases.^[59,63] We have double-checked that all homoepitaxial STO thin films are insulating after growth. Therefore, conductivity in the bilayers will be driven either by charge-transfer from the LAO layer or a redox-reaction starting from the interface (note that both processes are termination-sensitive as discussed in Ref. 30). An AFM image of amorphous LAO/STO/STO is presented in Figure S3 in the Supporting Information. The surface morphology shows distinct atomic step terraces, analogously to the case of crystalline LAO growth discussed in Figure 2. In **Figure 3**, we compare the temperature dependent transport properties of these LAO/STO/STO 2DEGs and the single crystalline standard case of the amorphous and crystalline LAO deposited directly on TiO₂-terminated substrates (LAO/STO). Regarding the temperature dependence of the sheet resistance, all samples show metallic behavior, both for the crystalline and amorphous case, and for LAO/STO and LAO/STO/STO (Figure 3a). At room temperature, the sheet resistance is similar for the two crystalline samples (light red/dark red) and for the two amorphous samples (light blue/dark blue) and all values are comparable to literature values of STO-single-crystal-based heterointerfaces.^[9,59] Interestingly, in the low temperature regime, the resistance achieved on STO thin films is about one magnitude higher than observed for STO single crystal samples. This confirms the assumption that the defect structures of the involved STO differ: At room temperature, the electronic transport properties are determined by the carrier formation process mainly, i.e. for charge-transfer interfaces (crystalline LAO) we

obtain similar conductivity, and for oxygen-vacancy-formation based interfaces (amorphous LAO) we obtain similar conductivity irrespective of having used a STO thin film or not, as long as the quality of the STO thin film allows the formation of a 2DEG. At low temperature, however, the electronic properties are apparently mainly governed by whether the STO is a thin film or a single crystal, i.e. in this temperature regime the two samples grown on single crystalline STO (crystalline & amorphous LAO) show similar conductivity, and the two samples grown on STO thin films

(crystalline & amorphous LAO) show similar conductivity. The conductivity of oxides in the low temperature regime is mainly influenced by scattering of electrons

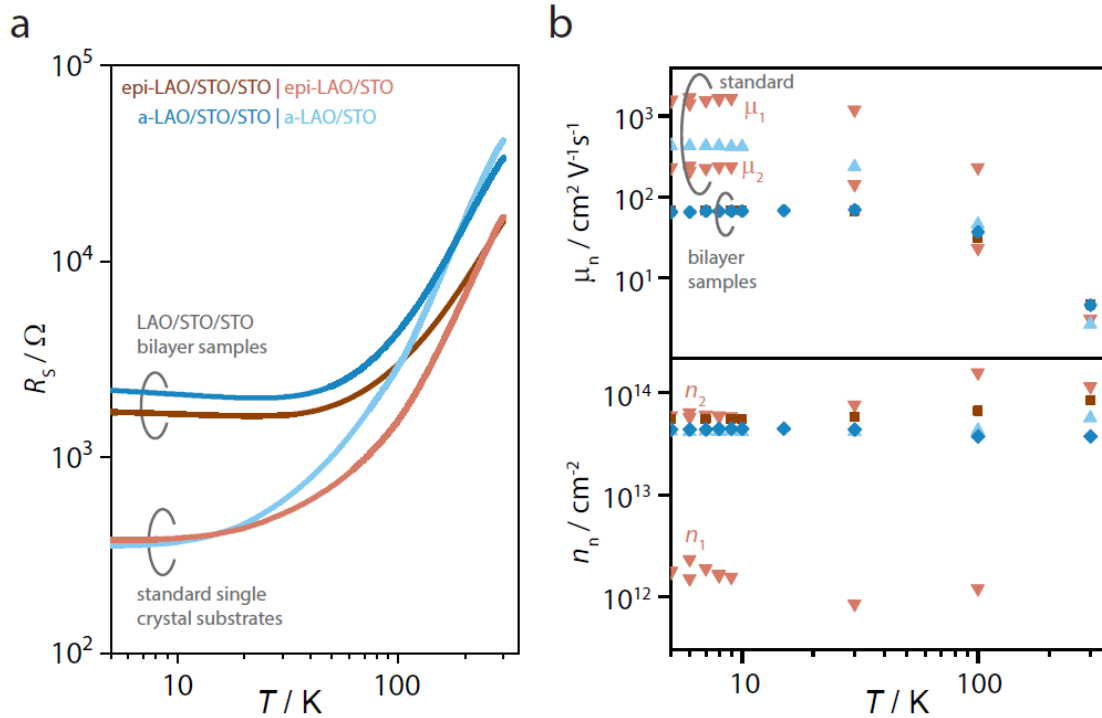


Figure 3. Electrical transport properties of 2DEGs generated at the interface of crystalline (reddish) and amorphous (blueish) LAO and STO thin film (epi-LAO/STO/STO and a-LAO/STO/STO (dark colors; squares)) or STO single crystal (epi-LAO/STO and a-LAO/STO (bright colors; triangles)). a) Sheet resistance, b) carrier density, and mobility in dependence of temperature. n_1 , n_2 and μ_1 , μ_2 used for epi-LAO/STO are carrier density and mobility obtained from multi-carrier model analysis. Note that the mobility values of epi-LAO/STO/STO and a-LAO/STO/STO are partially overlapping at low temperature.

on defects, which suggests that the increased resistance is due to a residual amount of defects, occurring at the interfaces to the STO thin film.

To get further information about the carrier types within those differently generated 2DEGs, we conducted Hall measurements in the low temperature regime and investigated the Hall resistance, R_{xy} . A linear Hall-effect was observed for all bilayer structures, which is different from the non-linear Hall effect typically observed in standard crystalline LAO/STO samples (See Figure S4 in the Supporting Information).^[19,64,65] The mobility and carrier density are extracted for all samples by fitting the Hall data, using a single-carrier model (for bilayers) and a multi-carrier model (in the reference sample) (Figure 3b).^[64] Consistently, the carrier concentration obtained for both bilayer conductive interface (5×10^{13} - 10^{14} cm⁻²) are of the same order as the carrier densities estimated from XPS results. As we observe a significant Ti³⁺ contribution, an average (volume) carrier density can be estimated of about 10^{20} cm⁻³ close to the interface. In this case, a 1-10 nm thick conductive layer will provide the vast majority of the electrons probed in transport (i.e. a sheet carrier density of 5×10^{13} - 10^{14} cm⁻²), which coincides well with the probed volume in XPS. This strongly suggest that the majority of carriers is close to the interface. In addition, at room temperature, the mobilities of LAO/STO/STO are similar to the ones on standard substrates and are similar for crystalline and amorphous LAO. At low temperatures, the mobilities of LAO/STO/STO become lower than the ones of LAO/STO but similar for crystalline and amorphous LAO. At low temperature, the extracted mobility (~ 70 cm²/Vs) for the interfaces generated on thin films is a factor

of 4-10 higher than the reported values (7-20 cm²/Vs) for samples, where LAO/STO interfaces are fabricated on various substrates and including PLD and MBE-grown STO.^[27,32,43] It is particularly interesting that the sheet carrier concentration is not influenced by the defects in the STO for both types of samples (amorphous and crystalline) (Figure 3b). However, the lowered mobility as compared to standard samples confirms that there is a residual amount of defects in the grown STO thin films and that the scattering mostly depends on the properties of the STO thin film. The same carrier density and altered mobility also implies that the scattering has little relation to the actual 2DEG formation process.

The lowered mobility in the bilayer sample also explains the absence of a non-linear Hall effect, which would be expected to be a general feature for any confined electron system in STO as a result of its complex band structure (*d*-band splitting).^[66] Experimentally, however, any charge carriers will only contribute to a non-linear field-dependence of R_{xy} if μB is close to unity. At a maximum field of about 10 T, typically applied in transport measurements, any charge carrier with $\mu < 100$ cm²/Vs, will hence not result in a non-linear Hall effect. In fact, a slightly reduced electron mobility as observed for the amorphous LAO/STO standard sample readily suppresses the non-linearity of the Hall effect as shown in Figure S4 in the Supporting Information. Assuming that mobility-ratios of high-mobility and low-mobility species is typically around 5,^[20,67] any low-mobility electron species present in the bilayer structures would not result in a significant non-linearity of the Hall effect. Therefore, the apparent linearity of the Hall effect is a direct result of a

residual disorder. Comparing with standard 2DEGs, the reduced mobility hence indicates a finite imperfection of the step-flow grown layers remaining even after improving and fine-adjusting the growth process. In turn, however, this residual imperfection may allow studying the magnetotransport in disordered, confined electron systems based on LAO/STO bilayer heterostructures. This is also a step towards transferring the interface to other materials and opens ways for fundamental studies on all-thin film heterointerfaces based on the improved STO growth process.

3. Conclusion

In summary, we demonstrated that the stoichiometry and termination of homoepitaxially grown STO thin films can be controlled by using high temperature growth and fine tuning of the laser fluence. Grown at 950°C with suitable laser fluence, STO thin films possess smooth surfaces, well-defined surfaces termination and low defect densities due to the step-flow growth mode. Fully metallic 2DEGs were observed at interfaces between both crystalline and amorphous LAO and grown STO thin film (200 nm). At low temperature (~2K), the stepflow-grown STO thin films yield a factor of 4-10 higher mobility than observed in comparable PLD and MBE LAO/STO-bilayer samples, as governed by the residual defect structure of the as-synthesized thin films.^[27,32,43] This in fact yields an opportunity to study disordered metallic systems based on LAO/STO bilayer heterostructures from a fundamental physics perspective, such as tunability of the defect structure as an option for novel functionality. Hereby, the results pave the way to design all-thin-film devices and transfer the LAO/STO bilayer to different substrates and heterostructures. Further, our

results are crucial for the realization of multiple conducting layers in superlattices or interfaces on other materials where exciting physical properties can be studied and also provides a basic for studies on back-gated all-thin-film devices.

4. Experimental Section

LAO and STO thin films were deposited by PLD with *in situ* RHEED monitoring. To grow films by PLD, substrates were attached to a resistive heater with silver paste and positioned 6.0 cm from the target. Single crystal STO target was ablated at varying total laser energy (adjusted by an attenuator at a given voltage), corresponding to F_L of 1.4 Jcm^{-2} to 4.0 Jcm^{-2} and a repetition rate of 5 Hz. The laser spot size on the target was fixed to $1.2 \times 10^{-2} \text{ cm}^2$ to avoid an additional impact of the spot size on the growth kinetics of STO thin films.^[68] Consequently, the growth rate shows a systematic dependence on the laser fluence, changing from 230 pulses per nanometer at the lowest laser fluence to about 80 pulses per nanometer at the highest applied laser fluence. Single crystal LAO target was ablated at a F_L of 2.4 Jcm^{-2} and a repetition rate of 1 Hz. The target-substrate distance was fixed at 6.0 cm. The STO films were grown on TiO_2 -terminated (001)-oriented STO single-crystalline substrates at temperatures ranging from 800 to 950 °C and an oxygen pressure of 0.13 mbar. Subsequently, the LAO layers were grown at 700 °C under an oxygen pressure of 1×10^{-4} mbar. After growth, the heterostructures were slowly cooled down to room temperature in the LAO deposition pressure at a rate of 10 °C/min, to allow oxygen equilibration of the heterostructures.^[69] Amorphous layers were deposited under similar conditions at room temperature. The structural quality of the samples was

analyzed by means of High-resolution XRD (HRXRD) system (*Bruker Discovery daVinci D8 DISCOVER*). It is equipped 2 bounced Ge (022) channel cut crystal for monochromatic X-ray beam which is $K_{\alpha 1}$ and the measurement have done around the STO (200) diffraction. AFM analysis was performed on a *SIS Pico Station UltraObjective* system in non-contact mode with a Si tip. The interfacial structure was characterized on cross-sectional samples prepared by focused ion beam milling using an *FEI Helios Nanolab 400s* dual-beam system and studied by HAADF STEM in an *FEI Titan G2 80-200 ChemiSTEM microscope*, equipped with a probe spherical aberration correction system and running at 200 kV. The electronic structure of the LAO/STO interfaces was determined by X-ray photoelectron spectroscopy (XPS) (Physical Electronics *PHI 5000 Versa Probe*) on the Ti 2*p* core level. The samples were illuminated with Al K_{α} X-ray illumination without charge neutralization, the analyzer pass energy was 58.7 eV and the photoemission angle was 0°. Fitting was performed using CasaXPS or using the peak models described in the main text using a Shirley background. Electrical transport properties were investigated with a Quantum Design Physical Property Measurement System (PPMS) from $T = 300$ K down to 2 K and an applied magnetic fields of $B = \pm 9$ T perpendicular to the interface. The samples were contacted in a mimicked Hall-bar geometry (inset in Figure 2c). The electrical contacts to the buried 2DEG layer were made by ultrasonic bonding with Al wires.

Supporting Information

Supporting Information is available from the Wiley Online Library or from the author.

Acknowledgments

H. Yan and J. M. Börger contributed equally to this work. H. Yan acknowledges the support from Sino-German (CSC-DAAD) Postdoc Scholarship Program, 2019 (201806290280). F. Gunkel and M. A. Rose thank the DFG GU/1604 (No. 315025796). C. Baeumer received funding from European Union's Horizon 2020 research and innovation programme under the Marie Skłodowska-Curie grant agreement No 796142.

Conflict of Interest

The authors declare no conflict of interest.

References

- [1] J. Mannhart, D. G. Schlom, *Science* **2010**, 327, 1607.
- [2] M. Bibes, A. Barthelemy, *IEEE Trans. Electron Devices* **2007**, 54, 1003.
- [3] N. A. Spaldin, R. Ramesh, *Nat. Mater.* **2019**, 18, 203.
- [4] F. Gunkel, D. V. Christensen, Y. Z. Chen, N. Pryds, *Appl. Phys. Lett.* **2020**, 116, 120505.
- [5] H. Y. Hwang, Y. Iwasa, M. Kawasaki, B. Keimer, N. Nagaosa, Y. Tokura, *Nat. Mater.* **2012**, 11, 103.
- [6] P. Zubko, S. Gariglio, M. Gabay, P. Ghosez, J. M. Triscone, *Annu. Rev. Condens. Matter Phys.* **2011**, 2, 141.
- [7] J. A. Mundy, Y. Hikita, T. Hidaka, T. Yajima, T. Higuchi, H. Y. Hwang, D. A.

- Muller, L. F. Kourkoutis, *Nat. Commun.* **2014**, 5, 3464.
- [8] M. Andrä, C. Funck, N. Raab, M. A. Rose, M. Vorokhta, F. Dvořák, B. Šmíd, V. Matolín, D. N. Mueller, R. Dittmann, R. Waser, S. Menzel, F. Gunkel, *Adv. Electron. Mater.* **2020**, 6, 1900808.
- [9] A. Ohtomo, H. Y. Hwang, *Nature* **2004**, 427, 423.
- [10] Y. Z. Chen, *Metal Oxide-Based Thin Film Structures*, **2018**, DOI:10.1016/b978-0-12-811166-6.00013-3283.
- [11] G. Herranz, M. Basletić, M. Bibes, C. Carrétéro, E. Tafr, E. Jacquet, K. Bouzehouane, C. Deranlot, A. Hamzić, J. M. Broto, A. Barthélémy, A. Fert, *Phys. Rev. Lett.* **2007**, 98, 216803.
- [12] A. Brinkman, M. Huijben, M. van Zalk, J. Huijben, U. Zeitler, J. C. Maan, W. G. van der Wiel, G. Rijnders, D. H. A. Blank, H. Hilgenkamp, *Nat. Mater.* **2007**, 6, 493.
- [13] N. Reyren, S. Thiel, A. D. Caviglia, L. F. Kourkoutis, G. Hammerl, C. Richter, C. W. Schneider, T. Kopp, A. S. Ruetschi, D. Jaccard, M. Gabay, D. A. Muller, J. M. Triscone, J. Mannhart, *Science* **2007**, 317, 1196.
- [14] J. Lee, A. A. Demkov, *Phy. Rev. B* **2008**, 78, 193104.
- [15] J. N. Eckstein, *Nat. Mater.* **2007**, 6, 473.
- [16] A. Kalabukhov, R. Gunnarsson, J. Börjesson, E. Olsson, T. Claeson, D. Winkler, *Phy. Rev. B* **2007**, 75, 121404.
- [17] P. R. Willmott, S. A. Pauli, R. Herger, C. M. Schleputz, D. Martoccia, B. D. Patterson, B. Delley, R. Clarke, D. Kumah, C. Cionca, Y. Yacoby, *Phys. Rev.*

- Lett.* **2007**, *99*, 155502.
- [18] A. S. Kalabukhov, Y. A. Boikov, I. T. Serenkov, V. I. Sakharov, V. N. Popok, R. Gunnarsson, J. Börjesson, N. Ljustina, E. Olsson, D. Winkler, T. Claeson, *Phys. Rev. Lett.* **2009**, *103*, 146101.
- [19] F. Gunkel, R. Waser, A. H. H. Ramadan, R. A. De Souza, S. H. Eifert, R. Dittmann, *Phys. Rev. B* **2016**, *93*, 245431.
- [20] F. Gunkel, C. Bell, H. Inoue, B. Kim, A. G. Swartz, T. A. Merz, Y. Hikita, S. Harashima, H. K. Sato, M. Minohara, S. H. Eifert, R. Dittmann, H. Y. Hwang, *Phys. Rev. X* **2016**, *6*, 031035.
- [21] L. Yu, A. Zunger, *Nat. Commun.* **2014**, *5*, 5118.
- [22] M. Andrä, H. Bluhm, R. Dittmann, C. M. Schneider, R. Waser, D. N. Mueller, F. Gunkel, *Phys. Rev. Mater.* **2019**, *3*, 044604.
- [23] Y. Z. Chen, F. Trier, T. Wijnands, R. J. Green, N. Gauquelin, R. Egoavil, D. V. Christensen, G. Koster, M. Huijben, N. Bovet, S. Macke, F. He, R. Sutarto, N. H. Andersen⁹, J. A. Sulpizio, M. Honig, G. E. D. K. Prawiroatmodjo, T. S. Jespersen, S. Linderöth, S. Ilani, J. Verbeeck, G. Van Tendeloo, G. Rijnders, G. A. Sawatzky, N. Pryds, *Nat. Mater.* **2015**, *14*, 801.
- [24] K. Han, K. Hu, X. Li, K. Huang, Z. Huang, S. W. Zeng, D. C. Qi, C. Ye, J. Yang, H. Xu, A. Ariando, J. B. Yi, W. M. Lü, S. S. Yan, X. R. S. Wang, *Sci. Adv.* **2019**, *5*, eaaw7286.
- [25] Z. Wang, Z. Chen, A. B. Mei, X. Bai, L. F. Kourkoutis, D. A. Muller, D. G. Schlom, *J. Vac. Sci. Techno. A* **2018**, *36* 021507.

- [26] M. L. R. Schmitt, C. Cancellieri, A. Cavallaro, G. F. Harrington, S. J. Leake, E. Pomjakushina, J. A. Kilner, P. R. Willmott, *Nanoscale* **2014**, 6, 2598.
- [27] J. W. Park, D. F. Bogorin, C. Cen, D. A. Felker, Y. Zhang, C. T. Nelson, C. W. Bark, C. M. Folkman, X. Q. Pan, M. S. Rzechowski, J. Levy, C. B. Eom, *Nat. Commun.* **2010**, 1, 94.
- [28] C. W. Bark, D. A. Felker, Y. Wang, Y. Zhang, H. W. Jang, C. M. Folkman, J. W. Park, S. H. Baek, H. Zhou, D. D. Fong, X. Q. Pan, E. Y. Tsybal, M. S. Rzechowski, C. B. Eom, *PNAS* **2011**, 108, 4720.
- [29] P. Brinks, W. Siemons, J. E. Kleibeuker, G. Koster, G. Rijnders, M. Huijben, *Appl. Phys. Lett.* **2011**, 98, 242904 .
- [30] F. V. E. Hensling, C. Baeumer, M. A. Rose, F. Gunkel, R. Dittmann, *Mater. Res. Lett.* **2020**, 8, 31.
- [31] M. L. R. Schmitt, C. Cancellieri, D. Li, D. Fontaine, M. Medarde, E. Pomjakushina, C. W. Schneider, S. Gariglio, Ph. Ghosez, J. M. Triscone, P. R. Willmott, *Nat. Commun.* **2012**, 3, 932.
- [32] F. Gunkel, S. Wicklein, S. H. Eifert, P. Meuffels, P. Brinks, M. Huijben, G. Rijnders, R. Waser, R. Dittmann, *Nanoscale* **2015**, 7, 1013.
- [33] N. Nakagawa, H. Y. Hwang, D. A. Muller, *Nat. Mater.* **2006**, 5, 204.
- [34] C. Baeumer, C. C. Xu, F. Gunkel, N. Raab, R. A. Heinen, A. Koehl, R. Dittmann, *Sci. Rep.* **2015**, 5, 11829.
- [35] G. Koster, B. L. Kropman, G. J. H. M. Rijnders, D. H. A. Blank, H. Rogalla, *Appl. Phys. Lett.* **1998**, 73, 2920.

- [36] D. J. Keeble, S. Wicklein, R. Dittmann, L. Ravelli, R. A. Mackie, W. Egger, *Phys. Rev. Lett.* **2010**, *105*, 226102.
- [37] R. Groenen, J. Smit, K. Orsel, A. Vailionis, B. Bastiaens, M. Huijben, K. Boller, G. Rijnders, G. Koster, *APL Mater.* **2015**, *3*, 070701.
- [38] T. Ohnishi, K. Takahashi, M. Nakamura, M. Kawasaki, M. Yoshimoto, H. Koinuma, *Appl. Phys. Lett.* **1999**, *74*, 2531.
- [39] Y. Kozuka, Y. Hikita, C. Bell, H. Y. Hwang, *Appl. Phys. Lett.* **2010**, *97*, 012107.
- [40] D. F. Li, S. Gariglio, C. Cancellieri, A. Fête, D. Stornaiuolo, J. M. Triscone, *APL Mater.* **2014**, *2*, 012102.
- [41] M. S. Li, Z. Huang, C. H. Tang, D. S. Song, T. P. Mishra, A. Ariando, T. Venkatesan, C. J. Li, S. J. Pennycook, *Adv. Funct. Mater.* **2019**, *29*, 1906655.
- [42] S. Thiel, C. W. Schneider, L. F. Kourkoutis, D. A. Muller, N. Reyren, A. D. Caviglia, S. Gariglio, J. M. Triscone, J. Mannhart, *Phys. Rev. Lett.* **2009**, *102*, 046809.
- [43] T. Hernandez, C. W. Bark, D. A. Felker, C. B. Eom, M. S. Rzchowski, *Phy. Rev. B* **2012**, *85*, 161407.
- [44] S. W. Zeng, X. M. Yin, T. S. Herng, K. Han, Z. Huang, L. C. Zhang, C. J. Li, W. X. Zhou, D. Y. Wan, P. Yang, J. Ding, A. T. S. Wee, J. M. D. Coey, T. Venkatesan, A. Rusydi, A. Ariando, *Phys. Rev. Lett.* **2018**, *121*, 146802.
- [45] D. Choe, M. J. Jin, S. I. Kim, H. J. Choi, J. Jo, I. Oh, J. Park, H. Jin, H. C. Koo, B. C. Min, S. Hong, H. W. Lee, S. H. Baek, J. W. Yoo, *Nat. Commun.* **2019**, *10*, 4510.

- [46] M. Kawasaki, K. Takahashi, T. Maeda, R. Tsuchiya, M. Shinohara, O. Ishiyama, T. Yonezawa, M. Yoshimoto, H. Koinuma, *Science* **1994**, 266, 1540.
- [47] D. J. Keeble, S. Wicklein, L. Jin, C. L. Jia, W. Egger, R. Dittmann, *Phys. Rev. B* **2013**, 87, 195409.
- [48] H. Y. Sun, Z. W. Mao, T. W. Zhang, L. Han, T. T. Zhang, X. B. Cai, X. Guo, Y. F. Li, Y. P. Zang, W. Guo, J. H. Song, D. X. Ji, C. Y. Gu, C. Tang, Z. B. Gu, N. Wang, Y. Zhu, D. G. Schlom, Y. F. Nie, X. Q. Pan, *Nat. Commun.* **2018**, 9, 2965.
- [49] Q. Y. Lei, M. Golalikhani, B. A. Davidson, G. Z. Liu, D. G. Schlom, Q. Qiao, Y. M. Zhu, R. U. Chandrasena, W. B. Yang, A. X. Gray, E. Arenholz, A. K. Farrar, D. A. Tenne, M. H. Hu, J. D. Guo, R. K. Singh, X. X. Xi, *npj Quant. Mater.* **2017**, 2, 10.
- [50] Y. F. Nie, Y. Zhu, C. H. Lee, L. F. Kourkoutis, J. A. Mundy, J. Junquera, P. Ghosez, D. J. Baek, S. Sung, X. X. Xi, K. M. Shen, D. A. Muller, D. G. Schlom, *Nat. Commun.* **2014**, 5, 4530.
- [51] S. Wicklein, A. Sambri, S. Amoruso, X. Wang, R. Bruzzese, A. Koehl, R. Dittmann, *Appl. Phys. Lett.* **2012**, 101, 131601
- [52] C. C. Xu, H. C. Du, A. J. H. van der Torren, J. Aarts, C. L. Jia, R. Dittmann, *Sci. Rep.* **2016**, 6, 38296.
- [53] J. Choi, C. B. Eom, G. Rijnders, H. Rogalla, D. H. A. Blank, *Appl. Phys. Lett.* **2001**, 79, 1447.
- [54] J. M. LeBeau, R. E. Herbert, B. Jalan, J. Cagnon, P. Moetakef, S. Stemmer, G. B. Stephenson, *Appl. Phys. Lett.* **2009**, 95, 142905.

- [55] S. A. Lee, H. D. Jeong, S. M. Woo, J. Y. Hwang, S. Y. Choi, S. D. Kim, M. S. Choi, S. K. Roh, H. S. Yu, J. S. Hwang, S. W. Kim, W. S. Choi, *Sci. Rep.* **2016**, *6*, 3649.
- [56] E. Breckenfeld, R. Wilson, J. Karthik, A. R. Damodaran, D. G. Cahill, L. W. Martin, *Chem. Mater.* **2012**, *24*, 331.
- [57] J. Lee, P. Jadhav, M. A. Baldo, *Appl. Phys. Lett.* **2009**, *95*, 033301.
- [58] S. Tanuma, C. J. Powell, D. R. Penn, *Surf. Interface Anal.* **1994**, *21*, 165.
- [59] Y. Z. Chen, N. Pryds, J. E. Kleibeuker, G. Koster, J. R. Sun, E. Stamate, B. B. Shen, G. Rijnders, S. Linderoth, *Nano Lett.* **2011**, *11*, 3774.
- [60] C. J. Li, Y. P. Hong, H. X. Xue, X. X. Wang, Y. C. Li, K. J. Liu, W. M. Jiang, M. R. Liu, L. He, R. F. Dou, C. M. Xiong, J. C. Nie, *Sci. Rep.* **2018**, *8*, 404.
- [61] Y. Z. Chen, D. V. Christensen, F. Trier, N. Pryds, A. Smith, S. Linderoth, *Appl. Surf. Sci.* **2012**, *258*, 9242.
- [62] A. Sambri, D. V. Cristensen, F. Trier, Y. Z. Chen, S. Amoruso, N. Pryds, R. Bruzzese, X. Wang, *Appl. Phys. Lett.* **2012**, *100*, 231605.
- [63] S. Thiel, G. Hammerl, A. Schmehl, C. W. Schneider, J. Mannhart, *Science* **2006**, *313*, 1942.
- [64] F. Gunkel, R. A. Heinen, S. H. Eifert, L. Jin, C. L. Jia, R. Dittmann, *ACS Appl. Mater. Interfaces* **2017**, *9*, 10888.
- [65] J. S. Kim, S. S. A. Seo, M. F. Chisholm, R. K. Kremer, H. U. Habermeier, B. Keimer, H. N. Lee, *Phys. Rev. B* **2010**, *82*, 201407.
- [66] A. F. Santander-Syro, O. Copie, T. Kondo, F. Fortuna, S. Pailhès, R. Weht, X. G.

- Qiu, F. Bertran, A. Nicolaou, A. Taleb-Ibrahimi, P. Le Fèvre, G. Herranz, M. Bibes, N. Reyren, Y. Apertet, P. Lecoeur, A. Barthélémy, M. J. Rozenberg, *Nature* **2011**, 469, 189.
- [67] H. J. H. Ma, Z. Huang, W. M. Lü, A. Annadi, S. W. Zeng, L. M. Wong, S. J. Wang, T. Venkatesan, Ariando, *Appl. Phys. Lett.* **2014**, 105, 011603.
- [68] H. N. Lee, S. S. A. Seo, W. S. Choi, C. M. Rouleau, *Sci. Rep.* **2016**, 6, 19941.
- [69] C. C. Xu, C. Bäumer, R. A. Heinen, S. H. Eifert, F. Gunkel, R. Dittmann, *Sci. Rep.* **2016**, 6, 22410.